

PERIODICO di MINERALOGIA  
established in 1930

*An International Journal of*  
*MINERALOGY, CRYSTALLOGRAPHY, GEOCHEMISTRY,*  
*ORE DEPOSITS, PETROLOGY, VOLCANOLOGY*  
and applied topics on *Environment, Archeometry and Cultural Heritage*

## Mineralogical and geochemical characterization of the concotto artefacts from firing places of Longola protohistoric settlement (Naples)

Giovanni Di Maio<sup>1</sup>, Giuseppina Balassone<sup>2,\*</sup>, Emhaie Ferrow<sup>3</sup>, Donatella Barca<sup>4</sup>, Angela Mormone<sup>5</sup>, Carmela Petti<sup>6</sup> and Nicola Mondillo<sup>2</sup>

<sup>1</sup> Geomed "Geoarchaeology and Environmental Geology" SRL, Via L. Sicignano, 84018 Scafati, Italy

<sup>2</sup> Dipartimento di Scienze della Terra, Università degli Studi di Napoli Federico II,  
Via Mezzocannone 8, 80134 Napoli, Italy

<sup>3</sup> Department of Earth and Ecosystem Sciences, Lund University, Sölvegatan 12, 223 62 Lund, Sweden

<sup>4</sup> Dipartimento di Scienze della Terra, Università della Calabria, Via P. Bucci, 87036 Rende, Italy

<sup>5</sup> Istituto Nazionale di Geofisica e Vulcanologia, Osservatorio Vesuviano, Via Diocleziano, 80124 Napoli, Italy

<sup>6</sup> Centro Museale "Centro Musei delle Scienze Naturali", Università degli Studi di Napoli Federico II,  
Via Mezzocannone 8, 80134 Napoli, Italy

\* Corresponding author: [balasson@unina.it](mailto:balasson@unina.it)

### Abstract

A set of concotto samples, a type of fired mixture of various raw materials, coming from firing place of the perfluvial protohistoric site of Longola (Campania region, southern Italy) was characterized by means of a multi-analytical approach, i.e. polarized light optical microscopy (OM), X-ray powder diffraction (XRD), scanning electron microscopy and energy dispersive spectrometry (SEM-EDS), X-ray fluorescence (XRF), inductively-coupled plasma-mass spectrometry (ICP-MS) and Mössbauer spectroscopy. The specimens generally show a heterogeneous texture, a red-coloured groundmass composed of a mixture of tiny quartz, feldspar, poorly-crystallized goethite, hematite and clay minerals. The crystal fractions show significant amounts of quartz and alkali feldspar and variable percentages of clinopyroxene, leucite, biotite, hematite, magnetite and traces of muscovite. Random secondary phases of calcite, vivianite and gypsum have been identified. The coarser fraction is formed by several types of inclusions, i.e. tephra fragments (pumices, scoriae), volcanic and sedimentary rocks. Illite and very subordinate smectite (montmorillonite) were detected by X-ray diffraction. Trace elements also show a contribution of volcanic raw materials. The Mössbauer analyses at 296 K show the occurrence of paramagnetic Fe<sup>3+</sup> iron (clay minerals) and magnetic Fe<sup>3+</sup> iron (hematite). For the 80 K spectrum, however, two doublets (ferrous and ferric iron in clay minerals) and one sextet (hematite). The concotto samples do not suffer high temperatures, perhaps much lower than 500-600 °C in a mainly oxidizing atmosphere. Only sporadically, if any, higher temperatures (> 800 °C) might have been reached.

*Key words:* concotto; archaeometry; Longola; southern Italy; protohistoric site; multi-technique investigations.

### Introduction

The Longola protohistoric village was discovered near to the townlet of Poggiomarino (Figure 1), east of Naples and northeast of Pompeii (southern Italy), in the year 2000, during the construction of a purification plant. It is located in the Sarno River Plain, more than seven

kilometers from the ancient river estuary. Its age spans from the late Middle Bronze Age to the 6<sup>th</sup> century B.C., when the site was definitely abandoned (Albore Livadie et al., 2010 and reference therein). This is a noteworthy discovery of a perifluvial settlement in southern Italy and in Europe, due to the peculiarity of its riverine location and the way in which it was constructed.

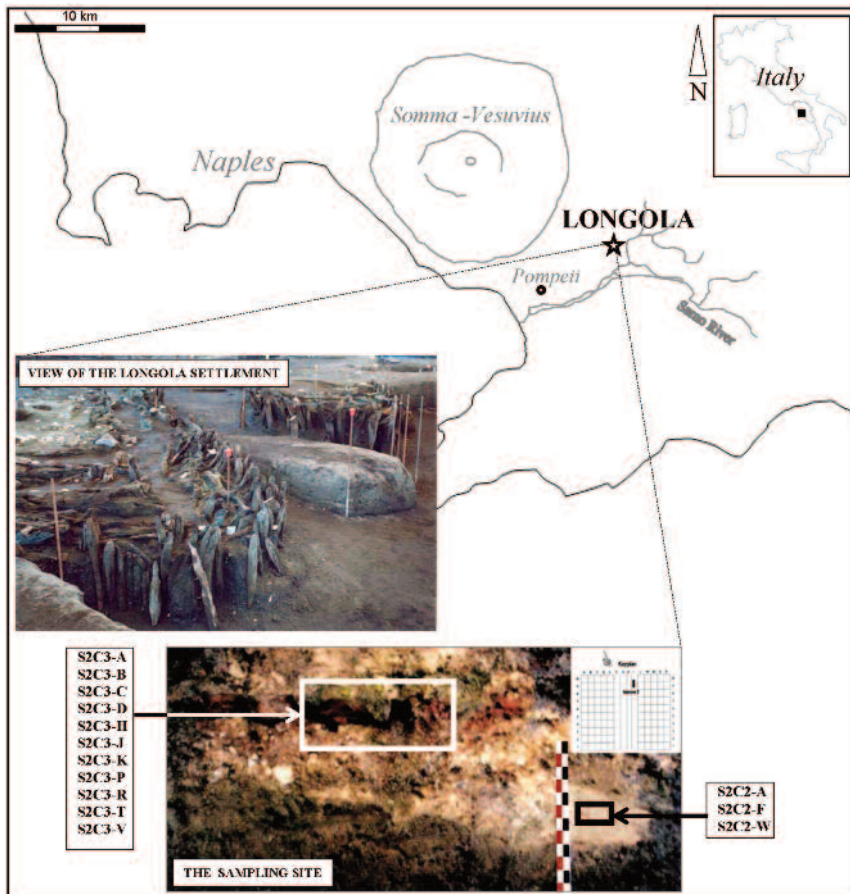


Figure 1. Schematic map of the study area, with a view of the Longola archaeological settlement and the sampling location (photos by G. Di Maio).

In fact the village was built on many artificial small islands surrounded by a navigable canal network; hence it has been surnamed “the prehistoric Venice”.

The Sarno River Plain is widely covered by the A.D. 79 and 472 eruptions of the Somma-Vesuvius, which contributed to the excellent preservation of the paleo-surface and the ancient paleo-environmental conditions before the eruption (Foss et al., 2002; Vogel and Märker, 2010). Numerous evidences of human activities, like houses, pirogues, numerous objects are present at Longola settlement. Handicraft working areas can be observed, where artefacts for domestic artisan and ornamental use were made. A great abundance of woods, ceramics and metallic objects (made of diversified materials like lead, bronze, iron and gold) has been found in the settlement, pointing to several distinct working/smelted sites throughout the village. In these working sites, fair evidences of heating have been detected on several materials (Cicirelli et al., 2006; Balassone et al., 2009a; Giachi et al., 2010). This is the first protohistoric perfluvial village discovered in southern Italy; in this area, other important archaeological sites, including the Roman “*Domus*” at Fontanelle and nearby necropolises, are currently under investigation.

In this paper, the compositional features of fourteen samples - likely used as coverings of burnt pavements, bricks or heat resistant vessel - coming from firing places found at Longola are characterized by means of a multi-analytical approach. As a matter of fact, the archaeometric studies successfully use integrated techniques typical of the geosciences to extract information from materials and objects of human activity and related palaeoenvironments (Maggetti, 2001; Maggetti and Messiga, 2006). The final research aim is to contribute in reconstructing the scenario of this Italian archaeological site by the knowledge of some production techniques, firing temperature estimate and provenance of raw materials.

### The archaeological site and sample description

The Longola settlement occurs in a wet environment strongly controlled by human activity and has been thoroughly investigated by drilling and digging of trenches. It has been inhabited from BM3 and the late Bronze Age (Albore Livadie and Cicirelli, 2003). Current investigations are concerned with the stratified sections belonging to the early Iron Age and to the Orientalizing period, until the early twenty years of the 6<sup>th</sup> century B.C.

The investigated artefacts mainly belong to a type of fired mixture of various raw materials called “*concotto*” by Italian archaeologists. Preliminary data on a batch of these specimens have been reported by Balassone et al. (2009b). These materials - used as bricks, oven walls, cooking wares, etc - are generally clayey and more or less friable to hard in consistence (Minguzzi et al., 1994; Bertelle et al., 2001).

The majority of the specimens studied are typically deep red to orange in colour with few specimens that show lighter colour ranging from reddish grey to creamy white (Table 1 and Figure 2). With the naked eye, the specimens studied show a heterogeneous texture consisting of a red-coloured groundmass containing variable amounts of microcrystalline phases, and inclusions of lithics (leucitic lava), pumices, scoriae, possible waste pottery and loose crystals (quartz, feldspar, clinopyroxene, leucite, and mica).

Locally whitish calcite-bearing crusts and veins and blue/black spots of vivianite can be detected. The samples resulted in fairly sturdy materials, particularly suitable for humid environments.

### Methods

The archaeometric investigation on the fourteen *concotto* samples was conducted by a multi-technique approach. Color, hardness and fabric were first described by visual examination.

Table 1. List of the samples analysed, with main macroscopic and some petrographic characteristics.

| Sample | Size (cm) | Macroscopic features   | Optical properties and grain sorting                              |
|--------|-----------|--|---|
| S2C2-A | 6 X 6     | light orange to creamy brown, fairly hard consistence                                  | isotropic matrix to locally anisotropic matrix, polymodal texture |
| S2C2-F | 4 X 5     | light orange to creamy brown, whitish parts, fairly hard material                      | isotropic matrix, polymodal texture                               |
| S2C2-W | 2 X 3     | red to creamy brown, white crusts, fairly hard material                                | isotropic matrix, polymodal texture                               |
| S2C3-A | 6 X 6     | red-orange, hard material with plane-parallel smoothed surfaces                        | isotropic to partly anisotropic matrix, polymodal texture         |
| S2C3-B | 5 X 5     | red-orange, hard material  | isotropic matrix, polymodal to bimodal texture                    |
| S2C3-C | 4 X 7     | red-orange, hard material  | isotropic matrix, polymodal texture                               |
| S2C3-D | 4 X 6     | red-orange, hard material  | isotropic matrix, polymodal texture                               |
| S2C3-H | 3 X 3     | red-orange, quite hard material  | isotropic matrix, polymodal texture                               |
| S2C3-J | 5 X 8     | red-orange, fairly hard material   | isotropic matrix, polymodal to bimodal texture                    |
| S2C3-K | 12 X 10   | red-orange, hard material with plane-parallel smoothed surfaces, rare black-blue spots | isotropic matrix, polymodal to bimodal texture                    |
| S2C3-P | 6 X 7     | red-orange, hard material  | isotropic matrix, polymodal texture                               |
| S2C3-R | 5 X 6     | red-orange with dark blue spots, hard material   | isotropic matrix, polymodal texture                               |
| S2C3-T | 4 X 4     | red-orange with dark blue spots and whitish crusts, hard material                      | isotropic to locally anisotropic matrix, bimodal texture          |
| S2C3-V | 3 X 5     | red-orange with black-blue spots, hard material with plane-parallel smoothed surfaces  | isotropic matrix, polymodal texture                               |

Polarized light optical microscopy (OM) on thin sections was used to characterize mineral phases and all the other components; modal analysis (Leica Qwin V3 Image Analyzer) was carried out on a minimum of 1000 points per slide in different random traverses to evaluate the relative percentages of inclusions, pores and groundmass for all the samples studied.

The mineral phases unidentifiable by OM were detected by means of X-ray powder diffraction (XRD), using a Seifert-GE MZVI diffractometer with a Cu K $\alpha$  radiation at 40kV and a 2 $\theta$  range of 3-70° with step size of 0.025° 2 $\theta$  and counting time of 5 s per step. The software package RayfleX (GE Inspection Technologies, 2004) was used for data processing and phase

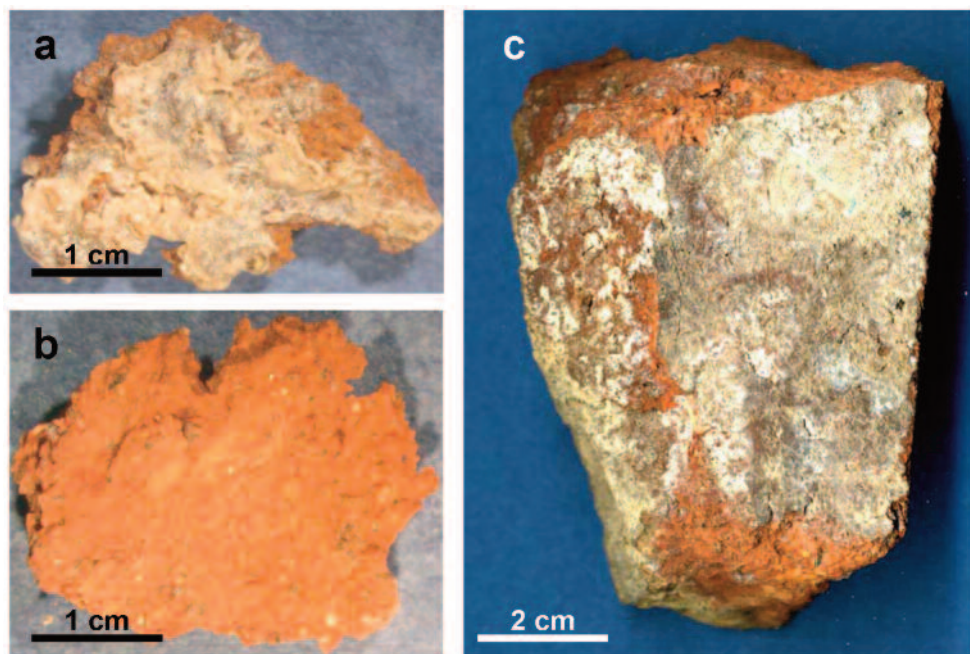


Figure 2. The typical concotto samples: a) S2C2-W; b) S2C3-H; c) S2C3-V (see Table1).

identification was made by means of the ICDD-PDF2 database. A minor set of XRD analyses were obtained using a Siemens D5000 diffractometer equipped with monochromatic Cu or Co  $K\alpha$ -radiation (Lund University, Sweden). The diffractograms were recorded between  $10^\circ$  and  $90^\circ$   $2\theta$  operating at 35 kV and 40 mA and with a scan speed of  $0.025^\circ$   $2\theta$   $\text{min}^{-1}$ .

Scanning electron microscopy (SEM) observations have been made by a JEOL JSM-5310 microscope (CISAG, University of Napoli Federico II) operating at 15 kV primary beam voltage, 50-100  $\mu\text{A}$  filament current and variable spot size and 50 s net acquisition time. Semi-quantitative and quantitative measurements of chemical composition were done with an energy dispersive spectrometry utilizing an Oxford Instruments Microanalysis unit, equipped with an INCA X-act detector and INCA X-stream pulse processor and using natural and synthetic

minerals as standards.

Whole rock major and trace element analyses have been performed in two laboratories. In the Department of Earth Science, University of Calabria (Italy), major and minor elements were determined by X-ray fluorescence (XRF) using a Bruker S8 Tiger spectrometer. The samples were ground to a fine powder in an agate mortar to prepare pressed pellets with boric acid as support. Accuracy was tested on international standards. The trace element concentrations were determined by using an ICP-MS system (Elan DRCe Perkin Elmer/SCIEX) by solution nebulisation. The powder was dissolved by microwave digestion using Mars5 microwave apparatus (CEM technologies). For each sample we prepared two diluted solutions (1/4 and 1/5) and we used as internal standard indium and germanium. The external calibration curves were prepared using Merck and Perkin Elmer standard

solutions. Standard reference materials were prepared in the same way and were used as unknown sample. The concentrations of the elements were compared with certified values to evaluate accuracy and precision of analytical data. While at ACME in Canada XRF, ICP and ICP-MS analyses, were performed on another sample batch using  $\text{LiBO}_2$  fusion and multi-acid digestion on 2 to 10 g of bulk samples.

The Mössbauer measurements were made with a 25 mCi  $^{57}\text{Co}$  source in an Rh matrix, which was driven at constant acceleration in a triangular mode. Mössbauer spectra were recorded at two temperatures (80 K and 296 K). Velocities were calibrated using Fe-foil with a thickness of 25  $\mu\text{m}$ . The spectra were computer-fitted and analysed using the Lorentzian site analysis in a commercially available Mössbauer spectral analysis software package. All isomer shift ( $\delta$ ) values are relative to  $\alpha$ -iron. As detailed by Wagner and Kyek (2004), the importance of superparamagnetism for the Mössbauer spectra of ceramics is by now well established. This is primarily due to the fact that the hematite formed during firing often has very small particle sizes ( $\geq 10 \leq 20$  nm). At room temperature and sometimes even down to quite low temperatures, the hematite nanoparticles exhibit fast superparamagnetic relaxations, which cause a collapse of the magnetic hyperfine sextet to a mere quadrupole doublet. If one wants to distinguish between superparamagnetic iron oxides, such as hematite, and paramagnetic structural iron in the silicates such as clay mineral, it is critical to cool the samples to liquid helium temperature or even lower, where superparamagnetism is usually blocked.

## Results

The mineralogical characterization has been made by combined optical microscopy (OM) and X-ray powder diffraction (XRD). In polarized light microscopy, with few exceptions, almost all

the samples have shown an isotropic groundmass (Figure 3). Their texture is mainly polymodal with the groundmass composed of a mixture of tiny quartz, feldspar, poorly-crystallized goethite, hematite and clay minerals. The crystal inclusions are represented by significant amounts of quartz and alkali feldspar, followed by variable percentages of clinopyroxene (salite to diopside), leucite, biotite, opaques (mainly hematite and magnetite) and traces of muscovite (Table 2a). Random secondary phases of calcite, vivianite and gypsum have been identified. Secondary calcite, locally containing up to 6% mol.  $\text{MgCO}_3$ , is detected in encrustations and veins and/or pore fillings. Vivianite occurs in several samples and in rather significant amount on the surfaces or in vugs of some of them. Gypsum is rarely found. The coarser granulometric fractions are formed by several types of inclusions, like tephra fragments (pumices, scoriae), volcanic rocks (leucite-bearing lava), sedimentary (Fe-oxi-hydroxides rich-, clayey, marly or carbonaceous) clasts, tiny ceramic shards (grog) and rare vegetable remains. An evaluation of the relative amounts of inclusions, groundmass and porosity of the Longola samples, based on modal data, is shown in Figure 4. The analysed samples are quite homogeneous in terms of percentages of inclusions - also referred as "packing" -, groundmass and porosity. Only samples no. S2C2-A, S2C2-F and S2C2-W, which are located in the lower part of the sampling site (see Figure 1), are characterized by a fairly higher porosity (8.8-9.1%), whereas in the other specimens pores are in the range 2.1-3.4%. The packing is between 27.4 and 35.2%, whereas the groundmass is in the range 59.6 and 70.7%.

Semi-quantitative mineralogical estimates was done by XRD (Table 2b). The prevailing quartz-feldspathic composition is confirmed and occurs in fairly homogeneous distribution in all samples. Clinopyroxene and iron oxihydroxides, i.e. hematite and goethite, are

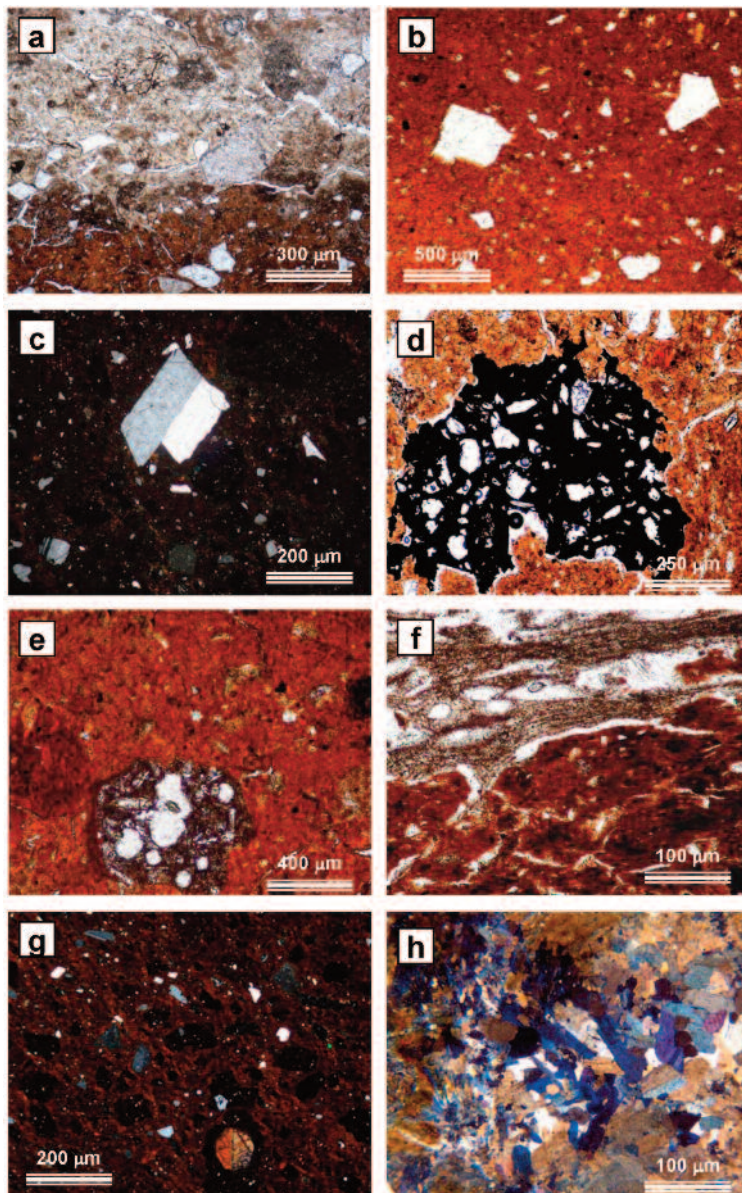


Figure 3. Thin section micrographs of selected sample. a) sample S2C2-F, quartz crystals and calcite-bearing crusts, parallel polars; b) sample S2C3-B, quartz grains in the red groundmass, parallel polars; c) sample S2C3-C, large Carlsbad twinned sanidine, with small quartz and plagioclase individuals, crossed polars; d) sample S2C3-E, scoria inclusion, parallel polars; e) S2C3-F, leucite-bearing lava lithic and goethite-rich, clay-rich and carbonatic small clasts, parallel polars; f) sample S2C3-T, vegetable remain, parallel polars; g) sample S2C3-D, quartz grains and a twinned clinopyroxene basal section, crossed polars; h) sample S2C3-V, vuggy vivianite crystals, parallel polars.

Table 2. (a) Percentages of inclusions (i.e. the total of crystals, scoriae, pumices and lithics), pores and groundmass evaluated by modal analysis of the Longola samples. (b) Their XRD semi-quantitative mineral composition (○○○○ = abundant, ○○○ = common, ○○ = quite common, ○ = scarce, x = traces, — = not detected).

| Sample | (a)*         |     |     |     |     |     |     |     |                                |     |                    |         | Pores | Ground-mass |  |
|--------|--------------|-----|-----|-----|-----|-----|-----|-----|--------------------------------|-----|--------------------|---------|-------|-------------|--|
|        | Inclusions** |     |     |     |     |     |     |     |                                |     | Scoriae<br>Pumices | Lithics |       |             |  |
|        | Qz           | Fsp | Cpx | Lct | Bt  | Ms  | Cal | Op  | Miscella-<br>neous<br>minerals |     |                    |         |       |             |  |
| S2C2-A | 10.0         | 4.7 | 0.5 | 1.1 | 0.8 | 0.1 | 2.0 | 0.7 | 0.7                            | 3.0 | 8.0                | 8.8     | 59.6  |             |  |
| S2C2-F | 11.3         | 5.0 | 0.1 | 0.4 | 0.3 |     | 1.9 | 0.5 | 0.5                            | 4.1 | 5.0                | 8.4     | 62.5  |             |  |
| S2C2-W | 14.7         | 4.4 | 0.9 | 0.1 | 0.2 |     | 1.8 | 0.5 | 0.3                            | 3.9 | 6.1                | 9.1     | 58.0  |             |  |
| S2C3-A | 13.9         | 8.0 | 1.0 | 0.1 | 0.9 |     |     | 0.7 | 0.3                            | 2.6 | 7.7                | 2.3     | 62.5  |             |  |
| S2C3-B | 14.2         | 4.3 | 0.3 | 0.1 | 0.2 | 0.1 | 1.2 | 1.1 | 0.5                            | 2.9 | 8.1                | 3.3     | 63.7  |             |  |
| S2C3-C | 13.7         | 3.9 | 0.3 | 0.1 | 0.2 |     |     | 1.0 | 0.6                            | 3.0 | 9.0                | 2.9     | 65.3  |             |  |
| S2C3-D | 10.2         | 4.1 | 0.2 | 0.1 | 0.4 |     | 0.3 | 1.1 | 0.6                            | 3.5 | 8.5                | 2.7     | 68.3  |             |  |
| S2C3-H | 13.7         | 4.0 | 0.4 | 0.1 | 0.3 |     |     | 1.2 | 0.5                            | 2.8 | 7.7                | 3.3     | 66.0  |             |  |
| S2C3-J | 10.0         | 5.0 | 0.2 | 0.1 | 0.2 |     | 2.9 | 1.3 | 0.9                            | 3.2 | 8.0                | 2.5     | 65.7  |             |  |
| S2C3-K | 15.1         | 8.5 | 0.1 | 0.1 | 1.0 |     | 1.1 | 1.0 | 0.5                            | 2.5 | 5.9                | 2.6     | 61.6  |             |  |
| S2C3-P | 13.9         | 5.1 | 0.1 | 0.1 | 0.1 |     | 0.8 | 1.2 | 0.4                            | 2.5 | 6.7                | 3.2     | 65.9  |             |  |
| S2C3-R | 14.0         | 3.8 | 0.8 | 0.1 | 0.3 |     | 1.0 | 0.5 | 0.2                            | 3.0 | 7.1                | 2.8     | 66.4  |             |  |
| S2C3-T | 10.6         | 4.2 | 0.9 | 0.1 | 0.9 |     | 0.1 | 1.1 | 0.4                            | 3.2 | 8.0                | 2.9     | 67.6  |             |  |
| S2C3-V | 11.0         | 4.0 | 0.8 | 0.1 | 0.2 |     | 0.1 | 0.6 | 0.4                            | 2.4 | 7.5                | 2.2     | 70.7  |             |  |

\* Percent errors: ± 5.6-5.8% (50-70%); ± 3.5-3.0% (8-15%); ± 2.0-2.5% (4-7%); ± 0.5-1.0% (1-3%); ± 0.1-0.3% (0.2-0.9%) ± 0.05% (0.1%).

\*\* Mineral (mostly after Whitney and Evans, 2010) and other abbreviations: Qz = quartz; Fsp = mainly alkali feldspar and minor plagioclase; Cpx = clinopyroxenes; Lct = leucite; Gth = goethite; Hem = hematite; Mag = magnetite; Bt = biotite; Ms = muscovite; Ill = illite; Sme = smectite; Cal = calcite; Gp Gypsum; Vvt = vivianite; Miscellaneous minerals = gypsum, goethite, clay minerals or vivianite; Lithics = lavas, sedimentary rock fragments, ceramic and vegetable remains.

ubiquitous, whereas magnetite is present in trace amounts. The dark mica is quite frequent, whereas low contents of muscovite occur only in four samples. Minor to trace amounts of clay minerals are also detected by X-ray diffraction and identified as mainly illite and smectite (montmorillonite).

Among the samples studied, it was only in sample S2C3-J that two small diffraction peaks, centred at 1.749 Å and 2.851 Å, were detected. They could possibly be assigned to traces of gehlenite (Ca<sub>2</sub>Al(AlSi)O<sub>7</sub>), a mineral of the

melilite group frequently occurring in archaeological ceramics and generally related to high-temperature firing processes (i.e. Maniatis et al., 1981; Cultrone et al., 2001; Barone et al., 2004; Grifa et al., 2009; Maggetti et al., 2011). Figures 5a and 5b show SEM micrographs of some parts of sample S2C3-J with evidences of a vitrification process; Figure 5c shows the two weak, not indexed, reflections in its XRD spectrum, tentatively given to gehlenite.

The bulk chemical composition of the samples was determined by XRF and ICP-MS and related

Table 2. Continued ...

| Sample | (b)  |     |     |     |     |     |     |    |    |     |    |     |     |     |
|--------|------|-----|-----|-----|-----|-----|-----|----|----|-----|----|-----|-----|-----|
|        | Qz   | Fsp | Cpx | Lct | Gth | Hem | Mag | Bt | Ms | Cal | Gp | Ill | Sme | Vvt |
| S2C2-A | ooo  | oo  | x   | o   | x   | x   | x   | o  | x  | o   | —  | o   | x   | —   |
| S2C2-F | ooo  | oo  | o   | x   | x   | x   | —   | x  | —  | o   | —  | x   | —   | x   |
| S2C2-W | oooo | oo  | o   | x   | x   | x   | x   | x  | —  | oo  | x  | o   | x   | —   |
| S2C3-A | oooo | ooo | o   | —   | o   | x   | —   | o  | —  | —   | —  | x   | —   | —   |
| S2C3-B | oooo | oo  | o   | —   | o   | o   | x   | —  | x  | o   | x  | o   | —   | x   |
| S2C3-C | oooo | oo  | o   | x   | o   | o   | x   | x  | —  | —   | —  | o   | —   | x   |
| S2C3-D | ooo  | oo  | o   | x   | oo  | o   | x   | —  | —  | x   | x  | o   | —   | x   |
| S2C3-H | oooo | oo  | o   | —   | o   | o   | —   | x  | —  | —   | —  | o   | —   | —   |
| S2C3-J | ooo  | oo  | o   | x   | o   | o   | x   | x  | —  | o   | x  | x   | —   | —   |
| S2C3-K | oooo | ooo | x   | —   | oo  | o   | —   | o  | —  | o   | —  | o   | —   | o   |
| S2C3-P | oooo | oo  | x   | x   | o   | o   | x   | x  | —  | o   | x  | x   | —   | x   |
| S2C3-R | oooo | ooo | o   | x   | oo  | x   | —   | —  | —  | o   | x  | o   | —   | o   |
| S2C3-T | ooo  | oo  | o   | —   | o   | o   | x   | o  | —  | —   | —  | o   | —   | x   |
| S2C3-V | ooo  | ooo | o   | x   | oo  | x   | x   | x  | —  | —   | —  | o   | —   | o   |

\*\* Mineral (mostly after Whitney and Evans, 2010) and other abbreviations: Qz = quartz; Fsp = mainly alkali feldspar and minor plagioclase; Cpx = clinopyroxenes; Lct = leucite; Gth = goethite; Hem = hematite; Mag = magnetite; Bt = biotite; Ms = muscovite; Ill = illite; Sme = smectite; Cal = calcite; Gp Gypsum; Vvt = vivianite; Miscellaneous minerals = gypsum, goethite, clay minerals or vivianite; Lithics = lavas, sedimentary rock fragments, ceramic and vegetable remains.

major and trace elements are reported in Table 3. The chemical behaviour of the samples analysed can be observed in diagrams for major and trace elements (Figure 6). The variability of silica, sodium, iron and titanium is moderate, showing a SiO<sub>2</sub> content in the range 46.86-56.76% wt.%, Na<sub>2</sub>O 0.59-1.73 wt.%, Fe<sub>2</sub>O<sub>3</sub> between 8.86 and 11.91 wt.%, TiO<sub>2</sub> between 0.71 and 1.28 wt.%. In contrast, CaO and K<sub>2</sub>O amounts vary to a larger extent, with the respective intervals between 2.04-7.55 wt.% and 3.05-10.24 wt.%. Indeed, the above mentioned sample S2C3-J is the richest in Ca, somehow supporting a possible

occurrence of gehlenite. Quite high P<sub>2</sub>O<sub>5</sub> amounts (1.11-4.26 wt.%) can be explained partly by the occurrence of vivianite. Compared to some Italian archaeological artefacts, like the *concotti* of Etrurian age from Marzabotto (Minguzzi et al., 1994) and bricks and kiln wastes of Roman age from *Caudium* (De Bonis et al., 2010), the studied specimens display an enrichment in iron, titanium and potassium and lower calcium contents (Figure 6a to 6d). The chemical trends of selected trace elements are shown in binary diagrams of Figure 6e and 6f. A quite homogeneous composition can be pointed

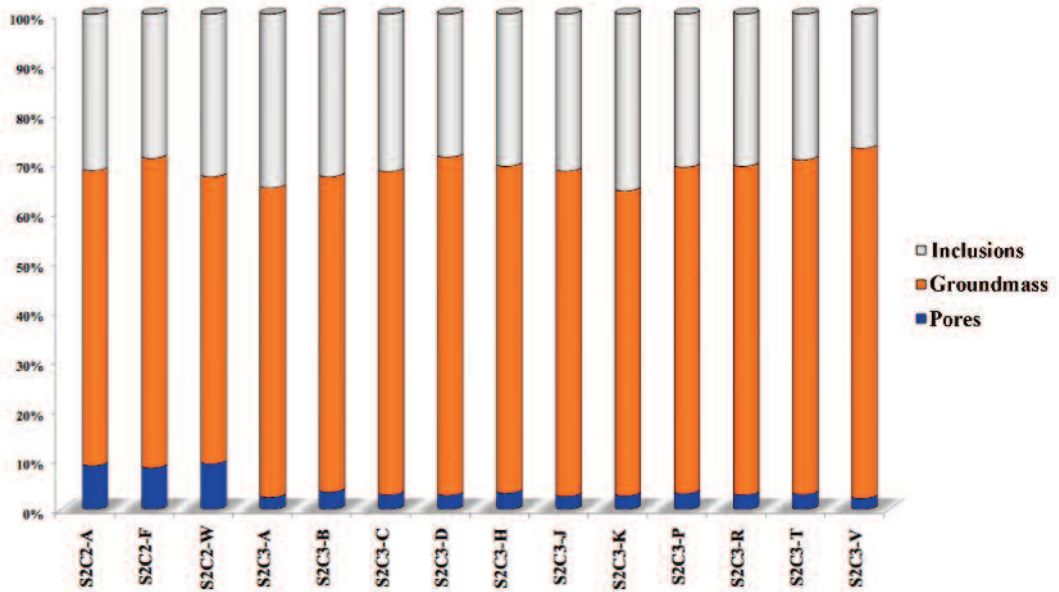


Fig 4. Relative abundances of inclusions, pores and groundmass estimated for the Longola samples by modal analysis (see Table 2a).

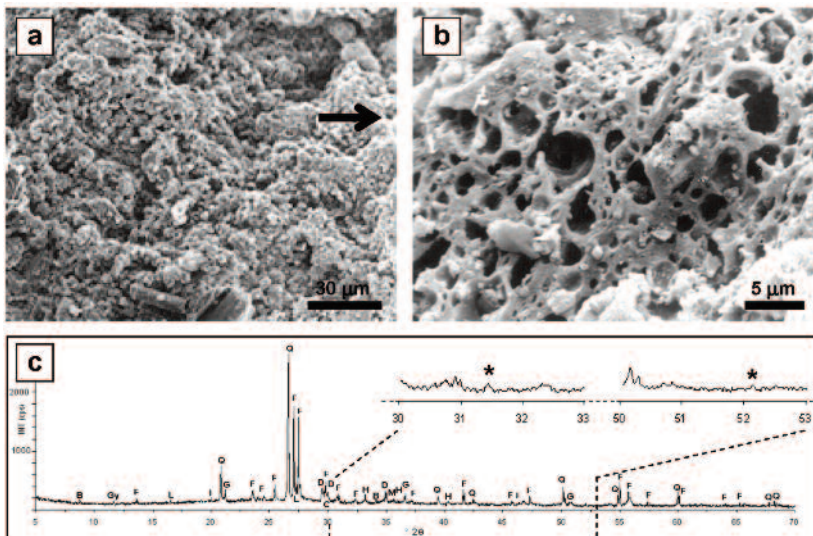


Figure 5. SEM micrographs and XRD diagram of sample S2C3-J. (a) groundmass and (b) enlargement (only partially indicated by the arrow in a) showing evidences of vitrification. (c) Diffraction pater in the range 5-70° 2θ (B, biotite; C, calcite; D, diopside; F, feldspar; G, goethite; Gy, gypsum; H, hematite; I, illite; L, leucite, M, magnetite; Q, quartz); on the top right side, the asterisks on the 30-33° to 50-53° 2θ ranges indicate two peaks possibly belonging to gehlenite.

Table 3. Major oxide (wt. %) and selected trace element (ppm) compositions of Longola samples, obtained by combined XRF, and ICP-MS analyses.

| Sample  | S2C2-A | S2C2-F | S2C2-W | S2C3-A | S2C3-B | S2C3-C | S2C3-D | S2C3-H | S2C3-J | S2C3-K | S2C3-P | S2C3-R | S2C3-T | S2C3-V |
|---|--------|--------|--------|--------|--------|--------|--------|--------|--------|--------|--------|--------|--------|--------|
| SiO <sub>2</sub>                              | 46.82  | 51.14  | 52.85  | 51.73  | 54.84  | 54.50  | 51.25  | 56.76  | 50.84  | 51.88  | 54.36  | 48.86  | 47.70  | 47.76  |
| TiO <sub>2</sub>                              | 0.71   | 0.82   | 1.02   | 1.00   | 1.04   | 0.98   | 1.28   | 0.85   | 0.99   | 0.93   | 1.03   | 1.03   | 1.15   | 1.03   |
| Al <sub>2</sub> O <sub>3</sub>                | 20.43  | 19.22  | 18.57  | 20.46  | 19.01  | 20.69  | 19.88  | 18.44  | 19.44  | 20.74  | 18.95  | 22.74  | 22.02  | 23.50  |
| Fe <sub>2</sub> O <sub>3</sub> <sub>tot</sub> | 9.69   | 8.86   | 10.02  | 9.46   | 10.52  | 10.35  | 11.09  | 9.18   | 9.99   | 9.34   | 10.54  | 8.88   | 10.89  | 11.91  |
| MnO   | 0.25   | 0.45   | 0.57   | 0.25   | 0.23   | 0.20   | 1.09   | 0.42   | 0.09   | 0.14   | 0.18   | 0.31   | 0.39   | 0.30   |
| MgO   | 2.54   | 3.67   | 4.12   | 4.13   | 2.18   | 3.92   | 2.67   | 5.12   | 3.30   | 3.08   | 2.71   | 4.47   | 5.34   | 3.59   |
| CaO   | 3.93   | 3.76   | 4.38   | 3.56   | 4.22   | 3.11   | 5.29   | 2.04   | 7.55   | 5.99   | 5.39   | 5.76   | 3.46   | 2.65   |
| Na <sub>2</sub> O                             | 1.73   | 1.56   | 1.27   | 1.02   | 1.51   | 1.17   | 1.32   | 1.11   | 1.39   | 1.38   | 1.55   | 0.65   | 0.97   | 0.59   |
| K <sub>2</sub> O                              | 10.24  | 6.24   | 4.47   | 6.31   | 4.47   | 3.50   | 3.90   | 4.07   | 4.60   | 5.22   | 4.18   | 5.83   | 6.06   | 6.34   |
| P <sub>2</sub> O <sub>5</sub>                 | 3.67   | 4.26   | 2.73   | 2.08   | 1.98   | 1.59   | 2.24   | 2.02   | 1.80   | 1.30   | 1.11   | 1.49   | 2.02   | 2.33   |
| LOI   | 100.00 | 100.00 | 100.00 | 100.00 | 100.00 | 100.00 | 100.00 | 100.00 | 100.00 | 100.00 | 100.00 | 100.00 | 100.00 | 100.00 |
| LOI   | 3.99   | 3.07   | 2.55   | 2.66   | 3.29   | 2.67   | 2.09   | 2.11   | 1.34   | 3.05   | 2.14   | 2.74   | 3.62   | 3.79   |
| S   | 82.0   | 178.7  | 300.0  | 709.9  | 900.6  | 1501.2 | 709.1  | 700.5  | 805.1  | 500.3  | 96.2   | 205.0  | 507.2  | 1477.0 |
| Cl  | 1449.0 | 1239.4 | 1253.2 | 367.7  | 400.4  | 437.2  | 417.1  | 612.4  | 700.2  | 911.2  | 745.3  | 304.0  | 433.8  | 414.0  |
| Sc  | 9.9    | 10.1   | 11.6   | 15.5   | 14.9   | 13.9   | 14.5   | 10.1   | 0.9    | 0.8    | 0.9    | 13.8   | 10.9   | 14.2   |
| V   | 136.9  | 133.9  | 159.8  | 175.1  | 176.6  | 169.8  | 170.9  | 151.4  | 88.1   | 67.3   | 121.2  | 162.6  | 167.3  | 179.8  |
| Cr  | 40.8   | 57.8   | 108.4  | 57.8   | 57.9   | 59.7   | 59.3   | 39.9   | 110.0  | 79.8   | 99.0   | 56.8   | 41.5   | 59.8   |
| Co  | 9.7    | 13.2   | 36.2   | 14.0   | 15.1   | 14.7   | 14.3   | 36.1   | 33.0   | 25.9   | 30.2   | 14.7   | 11.3   | 14.6   |
| Ni  | 30.0   | 33.3   | 29.6   | 58.4   | 60.7   | 56.7   | 48.2   | 41.4   | 28.4   | 35.0   | 71.0   | 38.1   | 39.4   | 41.7   |
| Cu  | 21.2   | 27.5   | 30.0   | 24.5   | 26.8   | 22.5   | 24.9   | 30.4   | 22.0   | 63.1   | 18.0   | 26.6   | 29.8   | 21.7   |
| Zn  | 104.6  | 111.2  | 76.0   | 203.8  | 225.7  | 260.9  | 187.2  | 114.7  | 58.0   | 99.0   | 270.0  | 149.7  | 121.9  | 268.2  |
| Rb  | 286.5  | 261.1  | 103.6  | 220.9  | 183.4  | 104.6  | 87.7   | 279.8  | 156.0  | 167.8  | 108.3  | 218.3  | 215.8  | 225.9  |
| Sr  | 273.5  | 299.5  | 400.2  | 409.6  | 421.3  | 334.9  | 350.1  | 389.0  | 376.0  | 445.0  | 399.0  | 360.1  | 466.0  | 312.4  |
| Y   | 30.9   | 26.7   | 25.3   | 44.1   | 45.8   | 46.7   | 41.3   | 40.1   | 54.3   | 45.2   | 29.2   | 41.5   | 37.5   | 46.4   |
| Zr  | 447.0  | 345.2  | 299.6  | 450.2  | 376.5  | 436.5  | 388.0  | 429.5  | 467.1  | 303.4  | 263.3  | 433.0  | 321.5  | 426.0  |
| Ba  | 357.1  | 355.7  | 287.5  | 444.6  | 443.9  | 453.2  | 437.2  | 422.3  | 499.8  | 500.2  | 200.3  | 450.0  | 447.1  | 431.3  |
| La  | 109.2  | 123.2  | 155.3  | 106.1  | 90.3   | 155.6  | 99.4   | 142.2  | 88.1   | 69.5   | 96.8   | 138.7  | 130.6  | 155.4  |
| Ce  | 165.2  | 145.1  | 122.3  | 196.2  | 190.8  | 187.8  | 200.1  | 167.7  | 99.0   | 168.5  | 89.8   | 187.3  | 178.3  | 198.2  |
| Pr  | 19.4   | 23.8   | 30.0   | 24.5   | 28.1   | 25.6   | 27.4   | 19.0   | 10.3   | 11.6   | 15.0   | 25.2   | 24.3   | 28.2   |
| Nd  | 72.3   | 87.9   | 100.2  | 99.9   | 110.9  | 113.5  | 98.6   | 109.8  | 102.9  | 158.6  | 85.9   | 97.3   | 99.9   | 111.1  |
| Sm  | 13.0   | 12.5   | 9.8    | 18.0   | 17.9   | 19.2   | 19.1   | 15.6   | 10.2   | 11.6   | 9.1    | 17.5   | 16.7   | 19.5   |
| Eu  | 2.2    | 3.3    | 3.9    | 3.0    | 3.0    | 3.0    | 3.5    | 2.0    | 2.1    | 3.6    | 2.1    | 3.0    | 3.1    | 3.3    |
| Gd  | 12.7   | 12.0   | 11.5   | 19.0   | 19.1   | 18.1   | 18.1   | 13.4   | 15.0   | 14.8   | 3.2    | 17.0   | 15.7   | 18.5   |
| Tb  | 1.3    | 1.4    | 1.8    | 2.0    | 1.9    | 1.8    | 2.1    | 2.0    | 1.4    | 2.1    | 1.2    | 1.7    | 2.0    | 1.9    |
| Dy  | 7.3    | 8.8    | 10.3   | 11.6   | 12.0   | 12.1   | 10.7   | 8.1    | 11.2   | 12.6   | 9.6    | 10.0   | 9.3    | 11.2   |
| Ho  | 1.2    | 1.5    | 1.6    | 1.7    | 2.0    | 1.6    | 1.9    | 2.0    | 0.9    | 1.8    | 1.4    | 1.6    | 1.8    | 1.8    |
| Er  | 4.0    | 4.4    | 5.0    | 3.9    | 4.5    | 6.7    | 5.0    | 4.0    | 3.1    | 3.9    | 5.6    | 5.4    | 5.2    | 6.0    |
| Tm  | 0.5    | 0.5    | 0.3    | 0.3    | 0.3    | 0.5    | 0.5    | 0.6    | 0.6    | 0.6    | 0.7    | 0.6    | 0.7    | 0.7    |
| Yb  | 3.8    | 4.3    | 4.6    | 4.9    | 4.7    | 5.2    | 6.1    | 4.9    | 4.8    | 5.1    | 5.1    | 5.2    | 5.3    | 5.7    |
| Lu  | 0.5    | 0.3    | 0.3    | 0.6    | 0.6    | 0.7    | 0.8    | 0.6    | 0.5    | 0.5    | 0.9    | 0.7    | 0.6    | 0.8    |
| Th  | 51.3   | 55.0   | 66.0   | 47.0   | 48.2   | 48.3   | 46.3   | 50.2   | 55.8   | 49.6   | 77.1   | 45.9   | 48.5   | 46.8   |
| Pb  | 59.4   | 78.1   | 89.0   | 130.4  | 131.3  | 129.9  | 130.9  | 129.7  | 186.2  | 200.5  | 136.2  | 77.0   | 128.5  | 129.1  |

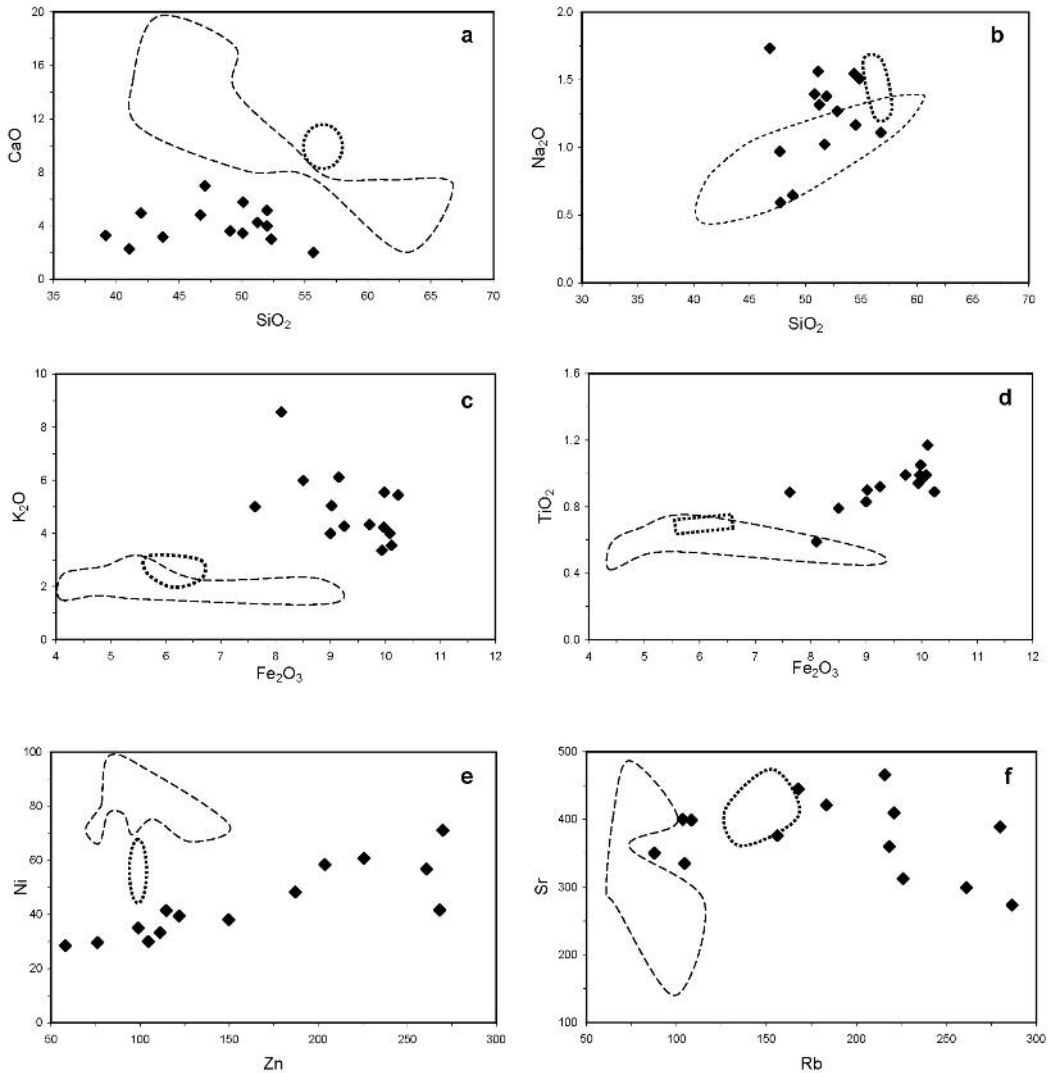


Figure 6. Selected major and trace element diagrams for the concotto samples. Dashed lines refer to Etrurian concotti from northern Italy (Minguzzi et al., 1994), dotted lines are related to fields of bricks and kiln wastes samples from Caudium, southern Italy (De Bonis et al., 2010).

out, making difficult to distinguish any grouping. From the comparison with the above mentioned occurrences, the values of the studied samples plot in different areas and show higher variability for Zn and Rb compositions.

For the sake of comparison, the behavior of Sr vs Zr in Somma-Vesuvius volcanic products with age greater A.D. 79 Pompeii eruption (Santacrose et al., 2008) and the Caudium archaeological specimens (De Bonis et al., 2010) is showed

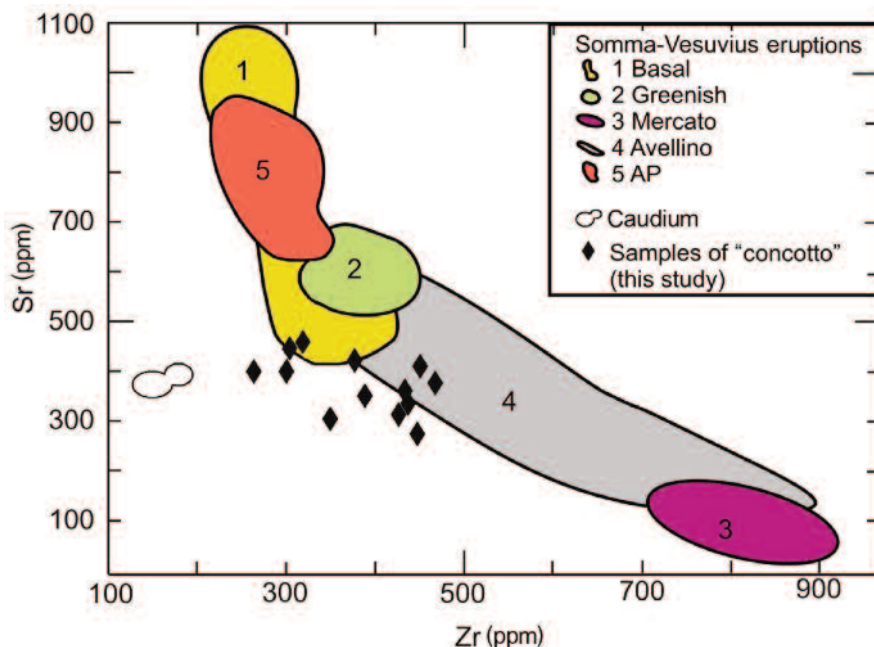


Figure 7. Zr vs Sr diagram for the studied *concocto* samples, compared to the compositions of major explosive eruptions of Somma-Vesuvius complex older than the AD 79 eruption (“Basal” = Pomici di base eruption, ca. 22000 yr. BP.; “Greenish” = Greenish Pumice eruption, ca. 19000 yr. BP.; “Mercato” = Mercato eruption, ca. 8900 yr. BP.; “Avellino” = Avellino eruption, ca. 3900 yr. BP.; “AP” = products between the Avellino and Pompeii eruptions.) and to the same Caudium samples of Figure 6 (De Bonis et al., 2010).

against the trend of the *concocto* samples in Figure 7. A contribution of volcanic raw material in the studied *impasti*, can be inferred (however, volcanics cropping out at Longola mainly belong to the Mercato eruption and to the protohistoric eruptive cycle).

Preliminary Mössbauer analyses have been performed for sample S2C3-K, considered representative of most of the samples for its macroscopic and microscopic features. Spectra - taken at 296 and 80 K - are plotted in Figure 8 and the corresponding Mössbauer parameters are listed in Table 4. For the 296 K spectrum only one doublet and one sextet are observed, the first for paramagnetic  $\text{Fe}^{3+}$  iron and the second for magnetic  $\text{Fe}^{3+}$  iron, respectively. The first is associated with the clay minerals and the second,

with magnetic field (H) close to 50 Tesla, is associated with hematite. For the 80 K spectrum, however, two doublets and one sextet are observed. The first doublet is due to ferrous iron in clay minerals, the second doublet due to ferric iron in clay minerals and the sextet due to hematite. Comparing the two spectra it can be concluded that the 80 K run shows sharper absorption lines resulting in well define lines for paramagnetic ferrous and ferric iron in clay minerals and a well defined sextet for hematite. The low temperature data gives a better distribution of the different iron species. The increase in intensity of ferric iron in hematite represents the presence of nanoparticles of hematite that were not identified at room temperature. The important problem of the

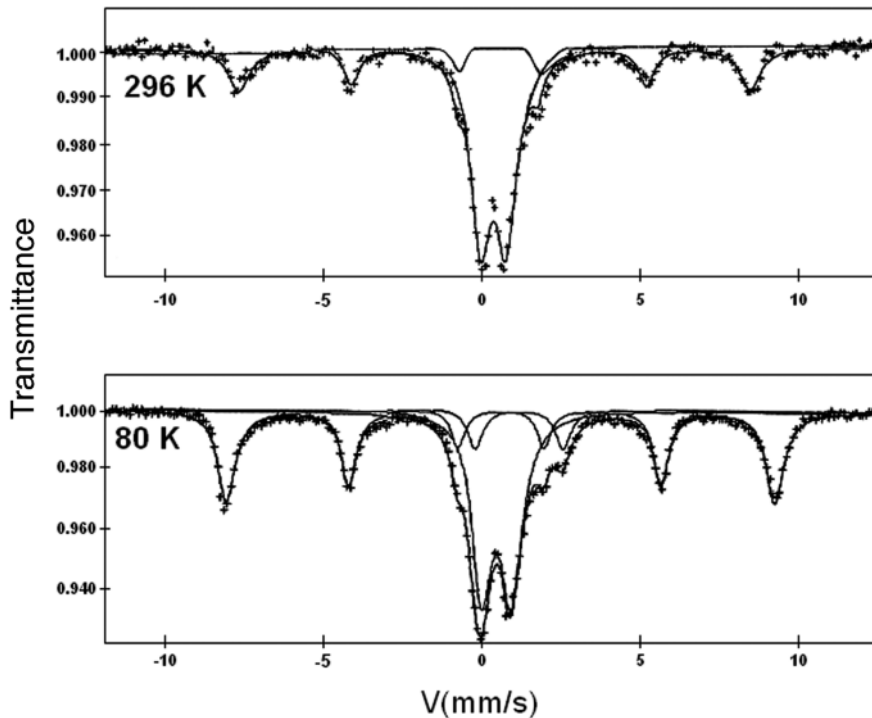


Figure 8. Mössbauer spectra of the sample S2C3-K, taken at 296 K and 80 K.

superparamagnetism of iron oxide nanoparticles, which causes collapse of hyperfine field splitting and loss of resolution for  $\text{Fe}^{2+}$  in room-temperature spectra, is solved in that all iron oxides and oxyhydroxides are hyperfine split at liquid helium temperature.

### Discussion and conclusions

Mineral composition can provide information on the firing techniques used, rough estimate on the prevailing thermal regime and on the redox of the environment. These combination of data can then be used to establish the technological know-how achieved by the ancient cultures.

The overall mineralogical, petrographic and geochemical data on the firing place artefacts from Longola have demonstrated their substantially

homogeneous feature, even if some differences can be pointed out.

The subset of samples S2C2-A, S2C2-F and S2C2-W shows a macroscopic lighter coloration and higher porosity. The discrete percentages of calcite and leucite - this latter as both loose crystals and lava lithics component of vesuvian provenance - can account for the higher Ca and K contents detected by whole rock analyses. A remarkable characteristic is the occurrence of montmorillonite in the samples S2C2-A and S2C2-W. Firing experimental works about the technological and mineralogical inferences on archaeological artefacts have found that this smectite is stable at temperature lower than 300 °C (Minguzzi et al., 1994; Fasani et al., 2006). Low firing temperatures, together with colour and porosity characteristics, can be in agreement

Table 4. Mössbauer parameters for a selected concotto sample (S2C3-K), taken at 296 and 80 K, respectively, for isomer shift (IS), quadrupole splitting for paramagnetic iron (QS) and for magnetic iron (e), line width (w), magnetic field (H), magnetic splitting (DH) and relative intensity (I).

|       |                  | IS   | QS/e | w     | H     | DH    | I     |
|-------|------------------|------|------|-------|-------|-------|-------|
|       |                  | mm/s | mm/s | mm/s  | Tesla | mm/s  | %     |
| 296 K | Fe <sup>3+</sup> | 0.36 | 0.81 | 0.79  |       |       | 68.10 |
|       | Fe <sup>3+</sup> | 0.36 | 0.10 | -0.10 | 50.35 | 16.24 | 31.90 |
| 80 K  | Fe <sup>2+</sup> | 1.11 | 2.75 | 0.57  |       |       | 8.16  |
|       | Fe <sup>2+</sup> | 0.47 | 0.92 | 0.78  |       |       | 49.14 |
|       | Fe <sup>3+</sup> | 0.48 | 0.07 | -0.07 | 52.98 | 17.09 | 42.70 |

with the peripheral position of the samples respect to the deep red-coloured samples in the site of the present study (Figure 1).

The batch of samples S2C3-A to S2C3-V has a slightly lower porosity and darker red colour. As in the above mentioned samples, the ubiquitous quartz and feldspar grains are associated with minerals deriving from the volcanic deposits of Somma-Vesuvius, always occurring both in the groundmass as single phases and in volcanic inclusions. Under optical microscope, diopside appears to be a detrital (volcanic) mineral, while no evidences of clinopyroxene neof ormation were pointed out. Taking into consideration that newly-formed diopside is a key-mineral for firing temperature constraints - indicating  $T > 850$  °C (Cultrone et al., 2001) - significant lower firing temperatures may be assumed for the site in this study. The lack of reaction margin in crystals and of primary calcite as well, together with the presence of illite, in the studied samples lead to suspect firing temperatures much lower than 800 °C. Just in one sample, a possible occurrence of newly formed gehlenite has been found, together with a vitrification evidence. Like diopside, this Ca-Al silicate is indicative of firing temperatures higher than 850 °C (Maggetti et al., 2011 and reference therein); then, a thermic variability within the same firing can be inferred, with only very

restricted areas of the investigated firing place having been subjected to locally higher temperatures. Besides, this is confirmed by ethno-thermometric data of Grosselain (1992); for archaeological open firings, he found a large temperature variability within the range 270-950 °C and also considerable variations in temperature in the same firing (or in the same pots), making it, in his opinion, impossible a true thermic characterization. Also burning experiments in open air conducted by Fasani et al. (2006) for archaeometric researches, confirm that great care is needed when seeking to extrapolate the actual kiln temperature during firings. In fact, according to these authors the mineral paragenesis stability indicates that the temperatures never exceed 450 °C. Ongoing optical microscopy and spectroscopic studies will further shed light on the firing temperatures of the Longola *concotti*.

<sup>57</sup>Fe Mössbauer spectroscopy, a technique specific for iron-bearing species, is of increasing usefulness for archaeologists, because can yield the possibility of inferring the conditions under which the minerals (clays and so on) were heated (Bertelle et al., 2001; Stievano et al., 2003; Ricciardi et al., 2008). On the basis of our preliminary <sup>57</sup>Fe Mössbauer data, the samples of the present work contain almost exclusively trivalent iron. In agreement with the study of Bertelle et al. (2001) on some protohistoric

concocto artefacts, firing in oxidizing conditions and an exposure of our concocto artefacts to relatively low temperatures, reached by firing in the open air, can be argue. This also agrees with the absence of neo-formed clinopyroxene. The small amount of  $\text{Fe}^{2+}$  that survives in the investigated specimens may again indicate an in situ heating in open air, at temperature lower than 800 °C, in such way that reduced iron can be preserved.

The variable amounts of secondary carbonate (calcite) and sulphate (gypsum) have been likely produced during burial, by concentration of carbonates dispersed in the burial environment as space fillings (Maggetti, 1994). Iron phosphate (vivianite) is generally considered a marker of a possible post-depositional contamination of phosphorous during burial, or is alternatively deposited starting from pre-existing P-rich matters, such as bones (Balassone et al., 1998; Maritan and Mazzoli, 2004). In our case, vivianite formation may be due to contamination after burial in environmental conditions of relatively low Eh and pH, because no bone accumulations have been found in the investigated site.

In conclusion, a possible scenario is that the concocto artefacts from Longola were formed by a mixture of local raw materials, of both volcanic and sedimentary/neoformed nature; they do not suffer high temperatures, likely lower than 500-600 °C in a mainly oxidizing atmosphere. Only very locally, if any, higher temperatures might have been reached.

### Acknowledgements

This paper is dedicated to the memory of Enrico Franco. We are indebted to the management of the *Soprintendenze Archeologiche* of Pompeii and Salerno for having allowed the sampling of the specimens for this study. This paper benefited from very helpful reviews by P. Mazzoleni (Università di Catania) and an anonymous reviewer and from the editorial advices of A. Gianfagna. The experienced assistance of R.

de Gennaro (CISAG Napoli) with the SEM-EDS analyses is acknowledged. M.C. Nanetti (Università di Bologna) is warmly thanked for bibliographic information. We also thank L.M. Francese and V. Monetti (Università di Napoli) for their technical assistance. Financial support to the present research came from Fund no. FS2/18/03 (Università di Napoli "Federico II") granted to G. Balassone.

### References

- Albore Livadie C. and Cicirelli C. (2003) - L'insediamento protostorico in località Longola di Poggiomarino - Nota Preliminare. In: Prima di Pompei. Un insediamento protostorico nel golfo di Napoli, Parola del Passato, Monografia Macchiaroli, 58, 88-128.
- Albore Livadie C., Castaldo E., Castaldo N., Cesarano B., Citro D., D'Avella A., Delle Donne M., Pappalardo M.T., Pizzano N. and Vannata R. (2010) - Le strutture abitative e di servizio dell'insediamento dell'età del ferro di Longola (Poggiomarino, Na). Atti Nono Incontro di Studi Preistoria e Protostoria in Etruria, Talentano (Vt), Pitigliano (Gr), 12-14 Settembre 2008, 539-551.
- Balassone G., Franco E. and Petti C. (1998) - La Campania antica. Dal Pleistocene all'Età Romana - Le analisi mineralogiche e petrografiche. Electa Napoli. 104-105.
- Balassone G., Boni M., Di Maio G. and Villa I.M. (2009a) - Characterization of metallic artefacts from the Iron Age culture in Campania (Italy): a multi-analytical study. *Periodico di Mineralogia*, 78, 45-63.
- Balassone G., Di Maio G., Barca D. and Mormone A. (2009b) - Archaeometric study of artefacts from firing places of Longola-Poggiomarino protohistoric settlement site (Naples, Italy). EGU General Assembly 2009, Wien, April 19-24, Vol. 11, 3486.
- Barone G., Crupi V., Galli F., Longo D., Majolino P., Mazzoleni P. and Spagnolo G. (2004) - Archaeometric analyses on 'Corinthian B' transport amphorae found at Gela (Sicily, Italy). *Archaeometry*, 46-4, 553-568.
- Bertelle M., Calogero S., Leotta G. and Stievano L. (2001) - Firing techniques of the Impasti from the protohistoric site of Concordia Sagittaria (Venice). *Journal of Archaeological Science*, 28, 197-211.
- Cicirelli C., Arbore Livadie C. and Boni M. (2006) -

- Dati preliminari sui manufatti metallici dell'insediamento protostorico in loc. Longola (Poggiomarino-Napoli). *Atti XXXIX Riunione Scientifica Istituto Italiano Preistoria e Protostoria "Materie prime e scambi nella preistoria italiana"*, I, 1391-1403.
- Cultrone G., Rodriguez-Navarro C., Sebastian E., Cazalla O. and De la Torre M.J. (2001) - Carbonate and silicate phase reaction during ceramic firing. *European Journal of Mineralogy*, 13, 621-634.
- De Bonis A., Grifa C., Langella A., Mercurio M., Perrone M.L. and Morra V. (2010) - Archaeometric study of roman pottery from Caudium area (Southern Italy). *Periodico di Mineralogia*, 79, 73-89.
- Fasani R., Basso E., Carò F., Cruciani G., Dalconi M.C., Ricciardi M.P. and Vecchi L. (2006) - Indagine archeometrica di strutture da fuoco provvisorie: la riproduzione sperimentale di una cottura "in buca". National Conference AiAr "Archeometria - Scienza e Beni Culturali", 1-3 February 2006, Pisa, Italy.
- Foss J.E., Timpson M.E., Ammons J.T. and Lee S.Y. (2002) - Paleosols of the Pompeii area. In: Jashemski W.F. (Ed.), *The Natural History of Pompeii*. Cambridge University Press, Cambridge, 66-79.
- GE Inspection Technologies (2004) - RayfleX. Version 2.336. GE Insp. Techn., USA-Germany.
- Giachi G., Mori Secci M., Pignatelli O., Gambogi P. and Mariotti Lippi M. (2010) - The prehistoric pile-dwelling settlement of Stagno (Leghorn, Italy): wood and food exploitation. *Journal of Archaeological Science*, 37, 1260-1268.
- Grifa C., Morra V., Langella A. and Munzi P. (2009) - Byzantine ceramic production from Cuma (Campi Flegrei, Napoli). *Archaeometry*, 51, 75-94.
- Grosselain O.P. (1992) - Bonfire of the enquiries. Pottery firing temperatures in Archaeology: what for? *Journal of Archaeological Science*, 19, 243-259.
- Maggetti M. (1994) - Mineralogical and petrographical methods for the study of ancient potter. In: Burrigato F., Grubessi O., Lazzarini L. (Eds), 1<sup>st</sup> European workshop of archaeological ceramics, Roma, 25-35.
- Maggetti M. (2001) - Chemical analyses of ancient ceramics: what for? *Chimia*, 55, 923-930.
- Maggetti M. and Messiga B. (2006) - Geomaterials in cultural heritage. *Geological Society, London*, 360 pp.
- Maggetti M., Neururer Ch. and Ramseyer D. (2011) - Temperature evolution inside a pot during experimental surface (bonfire) firing. *Applied Clay Science*, 53, 500-508.
- Maniatis Y., Simolopoulos A. and Kostikas A. (1981) - Mössbauer study of the effect of calcium content on iron oxide transformations in fired clays. *Journal of American Ceramic Society*, 64-5, 263-269.
- Maritan L. and Mazzoli C. (2004) - Phosphates in archaeological finds: implications for environmental conditions of burial. *Archaeometry*, 46, 673-683.
- Minguzzi V., Morandi N., Nanetti M.C., Trentini P., Mattioli C., Marchesi M. and Trocchi T. (1994) - Caratterizzazione minero-petrografica e studi termici di varie tipologie di "Concotto" di età etrusca (Marzabotto, BO). *Mineralogica Petrografica Acta*, 38, 219-227.
- Ricciardi P., Nodari L., Gualtieri S., De Simone D., Fabbri B. and Russo U. (2008) - Firing techniques of black lippe pottery from Nepal (12<sup>th</sup>-3<sup>rd</sup> century B.C.): the role of Mössbauer spectroscopy. *Journal of Cultural Heritage*, 9, 261-268.
- Santacroce R., Cioni R., Marianelli P., Sbrana A., Sulpizio R., Zanchetta G., Donahue D.J. and Joron J.L. (2008) - Age and whole rock-glass compositions of proximal pyroclastics from the major explosive eruptions of Somma-Vesuvius: A review as a tool for distal tephrostratigraphy. *Journal of Volcanology and Geothermal Research*, 177, 1-18.
- Stievano L., Bertelle M. and Leotta G. (2003) - Application of <sup>57</sup>Fe Mössbauer spectroscopy for the characterization of materials of archaeological interest: the work performer in Italy. *Hyperfine Interactions*, 150, 13-31.
- Vogel S. and Märker M. (2010) - Reconstructing the Roman topography and the environmental of the Sarno River Plain (Italy) before the A.D. 79 eruption of Somma-Vesuvius. *Geomorphology*, 115, 67-77.
- Wagner F.E. and Kyek A. (2004) - Mössbauer spectroscopy in Archaeology: Introduction and experimental considerations. *Hyperfine Interactions*, 154, 5-33.
- Whitney D.L. and Evans B.W. (2010) - Abbreviations for names of rock-forming minerals. *American Mineralogist*, 95, 185-187.